Observation of electron-hole cascade in photofield emission

P. J. Donders
Department of Physics, University of Toronto, Toronto, Ontario, Canada M5S 1A7

M. J. G. Lee
Department of Physics and Scarborough College, University of Toronto, Toronto, Ontario, Canada M5S 1A7

(Received 22 May 1989; revised manuscript received 31 August 1989)

Total energy distributions in photofield emission from single crystal planes of tungsten have been measured in *s*-polarized visible light. The strengths of the observed distributions, and their energy and electric-field dependences, are found to be consistent with the predictions of a simple model of field emission from an electron-hole cascade generated by the Auger decay of the photoexcited electrons. The results indicate that, well below the energy of the primary photoelectron peak, secondary electrons in the bulk metal make the dominant contribution to the emission current. Experimental observations in *p*-polarized light are also reported, and some possible interpretations are discussed.

I. INTRODUCTION

In a photofield emission (PFE) experiment, conduction electrons in the emitting metal are photoexcited to low-lying electronic states from where they may be field emitted either by passing above the peak of the Schottky potential barrier at the surface of the metal or by tunneling through it. PFE offers a means of studying the low-lying electronic states of the metal.

The incident light is characterized by the direction of the electric vector relative to the plane of incidence. If the electric vector is normal to the plane of incidence the illumination is said to be *s* polarized, whereas if the electric vector lies in the plane of incidence the illumination is said to be *p* polarized. Illumination at normal incidence is a special case of *s* polarization. The magnitude, energy dependence, and photon energy dependence of the emission current, are all found to be quite different for *s*- and *p*-polarized illumination. A study of the polarization dependence of PFE is of particular interest because in *s*-polarized light the emitted electrons are known to come from the bulk of the metal,[1] whereas in *p*-polarized light the emission current is dominated by electrons photoexcited at the emitting surface.[2]

The total energy distribution (TED) in PFE is approximately triangular in form when plotted on a semilogarithmic scale. At low energy, the energy dependence of the emission current is dominated by the exponentially decreasing probability of tunneling through the surface potential barrier, whereas at high energy the energy dependence is dominated by the exponential tail of the Fermi-Dirac distribution function that governs the occupation of initial states. In order to remove barrier transmission and thermal effects from the experimentally observed total energy distribution, and to emphasize those features that yield information about the electronic structure, it is usual to present the data by plotting the enhancement factor $R(E)$, which is defined by

$$R(E)\equiv\ln[j(E)/j_0(E)]\ , \tag{1}$$

where $j(E)$ is the observed total energy distribution, and

$$\begin{aligned} j_0(E)=&[m^3e\Omega^2/(2\pi^3\hbar^7)]f(E-\hbar\omega)[1-f(E)] \\ &\times|D|^2(E-\hbar\omega+V_0)^{1/2} \\ &\times\int_{-V_0}^{E}dW(W+V_0)^{-1/2}|T(W)|^2 \end{aligned} \tag{2}$$

is the total energy distribution of a noninteracting free-electron gas.[3] Here $f(E)$ is the Fermi-Dirac distribution function, $\hbar\omega$ is the photon energy, $|D|^2$ is the matrix element for optical transitions, W is the normal energy, V_0 is the magnitude of the potential step at the surface of the free-electron metal, $T(W)$ is the transmission amplitude at the surface potential barrier, and Ω is a normalizing volume. As the absolute quantum yield is not usually measured in a PFE experiment, the enhancement factor is determined only to within an additive constant.

The enhancement factor based on the noninteracting electron gas is appropriate so long as the flux of electrons at the emitting surface of the metal in the energy range of interest is dominated by primary photoelectrons. It is shown in this paper that in tungsten a significant fraction of the photoexcited electrons lose energy before being field emitted. Auger decay, in which quasiparticles lose energy by exciting electron-hole pairs, is the dominant inelastic scattering process. On the average each quasiparticle loses two-thirds of its excitation energy in each Auger event. Each Auger event yields three excited quasiparticles, and the quasiparticle lifetime varies inversely as the square of the excitation energy. Thus, Auger decay results in a cascade of low-energy electrons and holes in the vicinity of the Fermi level, significantly altering the energy distribution of the quasiparticle flux, and invalidating the definition of the enhancement factor based on the non-interacting electron gas.

This paper reports what is believed to be the first ob-

servation of photofield emission from an electron-hole cascade in tungsten, and shows how the enhancement factor for photofield emission must be modified to allow for this effect. In Sec. II the theory of the cascade is discussed, in Sec. III the experimental observation of the cascade is described, and in Sec. IV the results of the present work are discussed and the conclusions summarized.

II. AUGER DECAY OF PHOTOELECTRONS

An electron photoexcited within a bulk metal may reach the surface without being scattered, or it may experience one or more scattering events before reaching the surface. Scattering by the electron-phonon interaction results in only a small loss of energy (typically a few meV). By contrast, scattering by the electron-electron interaction leads to an energy loss that is typically a significant fraction of the excitation energy, and also results in the excitation of other electrons (i.e., secondary electrons) that may escape from the metal.

In photofield emission, the excitation energies $\varepsilon \equiv |E - E_F|$ of the primary electrons and primary holes (the latter cannot be observed directly) are typically in the range 2.0 to 3.5 eV. As the energies of the bulk and surface plasmons of tungsten (approximately 15 and 10 eV respectively[4]) are much larger than this, the excitation of real plasmons is not possible. In this situation, a photoelectron loses energy primarily by Auger decay, in which an electron-hole pair is excited in the Fermi distribution. Each member of the electron-hole pair is capable of exciting further electron-hole pairs, as illustrated in Fig. 1. Thus, the Auger decay of photoexcited electrons is expected to give rise to an electron-hole cascade, which greatly enhances the flux of electrons and holes with energies close to the Fermi level. Radiative transitions, which are strongly constrained by phase space considerations, are a much less probable mode of decay.

Wolff,[5] in a pioneering theoretical study of the electron-hole cascade, solved the Boltzmann transport equation for an excited electron in a free-electron gas, using interaction probabilities that were calculated by assuming a static two-body screened Coulomb interaction between the excited electron and an electron in the Fermi distribution. Since the work of Wolff, considerable progress has been made both in describing the interaction between electrons in solids,[6] and in calculating the resulting distributions of secondaries.[7]

Ritchie[8] has solved the set of transport equations that describe the decay of quasiparticles in a homogeneous free-electron gas in the low density limit. Adopting Ritchie's notation, let the normalized electron excitation energy be $x \equiv \varepsilon_e / E_F$ and let the normalized hole excitation energy be $y \equiv \varepsilon_h / E_F$ (both x and y are positive). The probabilities of interaction for the various decay processes are required. $\mu_{e1}(x,x')$ is the probability (per unit energy range per unit path length) of the direct decay of an electron from an initial state of energy x to a final state of energy x', accompanied by the excitation of an electron-hole pair from the Fermi distribution to conserve energy, and $\mu_{e2}(x,x')$ is the probability of the corresponding process in which the electron that is excited from the Fermi distribution has a final state of energy x'. $\mu_{e\text{-}h}(x,y)$ is the probability that the Auger decay of an electron from an initial state of energy x yields a final-state hole of energy y. Similarly, $\mu_{h1}(y,y')$ is the probability (per unit energy range per unit path length) of the direct decay of a hole from an initial state of energy y to a final state of energy y', accompanied by the excitation of an electron-hole pair, and $\mu_{h2}(y,y')$ is the probability of the corresponding process in which the hole that is excited from the Fermi distribution has a final state energy y'. $\mu_{h\text{-}e}(y,x)$ is the probability that the Auger decay of a hole from an initial state of energy y yields a final state electron of energy x.

A calculation based on the Lindhard theory of the dielectric function[9] of an interacting free-electron gas yields the following approximate expressions for these probabilities in the limit $(x,y) \ll 1$:

$$\begin{aligned} &\mu_{el}(x,x') = \mu_{e2}(x,x') = \mu_0(x - x')\Theta(x - x') , \\ &\mu_{eh}(x,y) = \mu_0(x - y)\theta(x - y) , \\ &\mu_{hl}(y,y') = \mu_{h2}(y,y') = \mu_0(y - y')\Theta(y - y') , \\ &\mu_{he}(y,x) = \mu_0(x - y)\Theta(y - x) . \end{aligned} \tag{3}$$

In these expressions, $\Theta(z)$ is the unit step function, μ_0 is an inverse screening length defined by

$$\mu_0 \equiv (1/8\gamma a_0)[\tan^{-1}(1/\gamma) + \gamma/(1+\gamma^2)] , \tag{4}$$

a_0 is the Bohr radius, and $\gamma \equiv (4/9\pi^4)^{1/6} r_s^{1/2}$. r_s, a dimensionless measure of the density of the electron gas, is defined as the radius of the sphere that on the average contains just one electron, expressed in units of a_0.

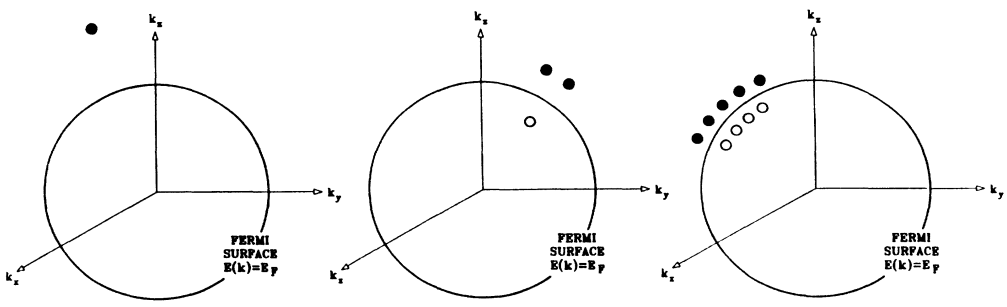

FIG. 1. Illustration of the electron-hole cascade in momentum space.

Using these interaction probabilities, and assuming electron-hole number balance (thereby neglecting radiative decay) Ritchie solved the set of transport equations for the case of a monoenergetic steady uniform source generating one electron of energy x_0 per unit volume per unit time per unit energy interval in a free-electron gas.[8] In the limit where the excitation energy is much less than the Fermi energy, Ritchie's expressions yield a steady-state electron flux given by

$$\mu(x)=\frac{6}{0.5\mu_0 x_0^3}\left\{\left[\frac{x_0}{x}\right]^4-\frac{x}{x_0}+\frac{5}{9}\left[\left[\frac{x_0}{x}\right]^3-1\right]\right\}+\frac{2}{\mu_0 x_0^2}\delta(x-x_0)\ , \tag{5}$$

and a steady-state hole flux given by

$$v(y)=\frac{6}{5\mu_0 x_0^3}\left\{\left[\frac{x_0}{y}\right]^4-\frac{y}{x_0}-\frac{5}{9}\left[\left[\frac{x_0}{y}\right]^3-1\right]\right\}. \tag{6}$$

The flux of primary electrons, the delta function term in Eq. (5), varies as x_0^{-2}, reflecting the fact that the number of electrons with which a given primary electron can interact, and hence the rate of scattering of primary electrons, is proportional to x_0^2. As the excitation energy approaches zero, the flux of secondary electrons and secondary holes diverges as the inverse fourth power of the excitation energy. The extension of Eqs. (5) and (6) to describe the decay of energetic holes is accomplished by interchanging the roles of x and y.

Kane[10] has carried out a calculation of the Auger decay of excited electrons in silicon based on a realistic treatment of the electronic structure, in which the dielectric function was evaluated in the random-phase approximation. The summation over all transitions in which an excited electron with energy and momentum $(x,\mathbf{k}_e)$ decays to state $(x',\mathbf{k}_e')$, creating an electron-hole pair in states $(x'',\mathbf{k}_e'')$ and $(y'',\mathbf{k}_h'')$, was performed by the Monte Carlo method. The precision of such calculations is limited by the time required to identify transitions that conserve both energy and momentum.

Kane also investigated the random-**k** approximation, in which momentum conservation and matrix element effects are neglected. Then the interaction probabilities of Eq. (3) are replaced by

$$\begin{aligned}
&\mu_{el}(x,x')-\mu_{e2}(x,x')=\gamma\rho(x')\int dx''\rho(y'')\rho(x'')\delta(x-x'-x''-y'')\ ,\\
&\mu_{eh}(x,y)=\gamma\rho(y)\int dx''\rho(x')\rho(x'')\delta(x-y-x'-x'')\ ,\\
&\mu_{hl}(y,y')=\mu_{h2}(y,y')=\gamma\rho(y')\int dy''\rho(x'')\rho(y'')\delta(y-y'-y''-x'')\ ,\\
&\mu_{he}(y,x)=\gamma\rho(x)\int dy''\rho(y')\rho(y'')\delta(y-x-y'-y'')\ ,
\end{aligned} \tag{7}$$

where $x,x',x'',y,y',y''>0$, γ is a constant, and where the δ functions conserve energy. Kane found that this much simpler calculation essentially reproduces the results of the full Monte-Carlo calculation.

In photofield emission in *s*-polarized light, the absorption of a photon creates an electron-hole pair within the bulk metal. Each of the quasiparticles decays *via* interactions with the other electrons. In typical conditions, the barrier transmission probabilities of the vast majority of the photoexcited electrons are much less than unity. Moreover, the penetration depth of the incident light is typically ~200 Å, which is larger than the mean free paths of the quasiparticles (30 to 150 Å in this energy range[11]). It follows that the steady state flux of electrons and holes at the emitting surface is representative of the electron-hole cascade in the bulk metal.

Ritchie's results may be applied to calculate the TED for photofield emission in *s* polarization from an interacting electron gas. If the photoexcitation probability is assumed to be independent of the initial and final states involved, and the electron velocity is assumed to be independent of excitation energy, then in the energy range $0<E-E_F<\hbar\omega$ the predicted TED at $T=0$ K will be of the form

$$j_0^*(E)\propto s\left[\frac{E-E_F}{\hbar\omega}\right]\int_{-V_0}^{E} dW(W+V_0)^{-1/2}|T(W)|^2\ , \tag{8}$$

where

$$s(z)=\frac{1}{5}\left[\frac{3}{z^4}+2z\right]. \tag{9}$$

Comparison with Eq. (2) shows that, in the limit of a noninteracting electron gas, the temperature dependence of the TED is calculated by multiplying the integrand by the Fermi-Dirac distribution function $f(E-\hbar\omega)$. Only close to the peak of the photoelectron distribution $(E\sim E_F+\hbar\omega)$ does the emission current depend significantly on temperature. In the presence of interactions, emission from close to the peak of the photoelectron distribution is dominated by primary photoelectrons. Hence at finite temperature the TED in the interacting free-electron gas can be calculated to a good approximation by multiplying the integrand in Eq. (7) by the Fermi-Dirac distribution function $f(E-\hbar\omega)$.

Over the energy range from $\hbar\omega/6$ to $\hbar\omega$, the coefficient multiplying the integral in Eq. (2) (for the noninteracting electron gas) increases by a factor of 1.2, while the coefficient multiplying the integral in Eq. (8) (for the interacting electron gas) decreases by a factor of approximately 800. Hence, the energy dependence of the TED of the interacting electron gas is very different from that of the noninteracting electron gas. Secondary electrons are expected to make the dominant contribution to the total energy distribution at energies less than $\hbar\omega/2$.

A more realistic model would require a treatment of the electronic structure of the field emitter. A calculation based on the random-**k** approximation of Kane has been carried out to test whether departures from a free-electron band structure must be taken into account when calculating the steady state distribution of secondary electrons.

III. EXPERIMENT

The experimental apparatus for measuring total energy distributions in photofield emission has been described elsewhere.[12] The features of the apparatus that are essential for the success of the present experiments are an energy analyzer capable of high resolution and facilities for measuring photofield emission TED's with illumination at normal incidence.

Photofield emission TED's for tungsten were recorded at each desired photon energy using a computer-controlled data acquisition system. The distribution was divided into 100 equal channels, each having a width of 25 mV. The tip was cleaned by flashing to white heat, and then the entire distribution was collected every 200 ms by sweeping through the channels sequentially and recording the counts accumulated in each channel in 2.0 ms. To monitor the background signal, the TED's were acquired in pairs, one TED with the tip illuminated and the other with the laser beam blocked. Acquisition of the two TED's was interleaved in time, with a cycle time of about 40 sec, in order to average out the effects of drift and gradual tip contamination. Typically it took from 20 to 40 min to accumulate a complete set of data, during which time the drift in the total photocurrent was less than 10%. However, the emission current from the W(211) plane was found to decrease by approximately 50% in 30 min, because the work function of this plane is very sensitive to tip contamination. Therefore, the tip was cleaned at 4 min intervals during data acquisition from the (211) plane.

The high-energy tail of the TED in field emission from the illuminated tip was estimated by correcting the TED measured in the absence of illumination for the temperature rise caused by illuminating the tip. The strength of the low-energy tail due to inelastic scattering within the energy analyzer was estimated by appropriately scaling the corresponding tail of the TED in field emission from the unilluminated tip. The TED in photofield emission was deduced by subtracting these corrections from the TED from the illuminated tip.

Several distinct effects contribute to the shape of the TED measured in the absence of illumination, as illustrated in Fig. 2. The component labeled A, which is due to field emission from thermally populated electronic states of the metal, exhibits a characteristic exponential energy dependence. The component labeled B, a high-energy tail in the field emission TED, is caused by Coulomb scattering between electrons just outside the emitting plane of the field emitter.[13] The strength of component B is proportional to the square of the total field emission current, and the current density exhibits an $(E-E_F)^{-2.6}$ energy dependence over the range of interest. The remaining component, labeled C, represents field emitted electrons that reach to detector after scattering from the walls of the energy analyzer. Since the background due to electron multiplier noise is negligible (less than 1% of the minimum signal), this contribution is not indicated in Fig. 2.

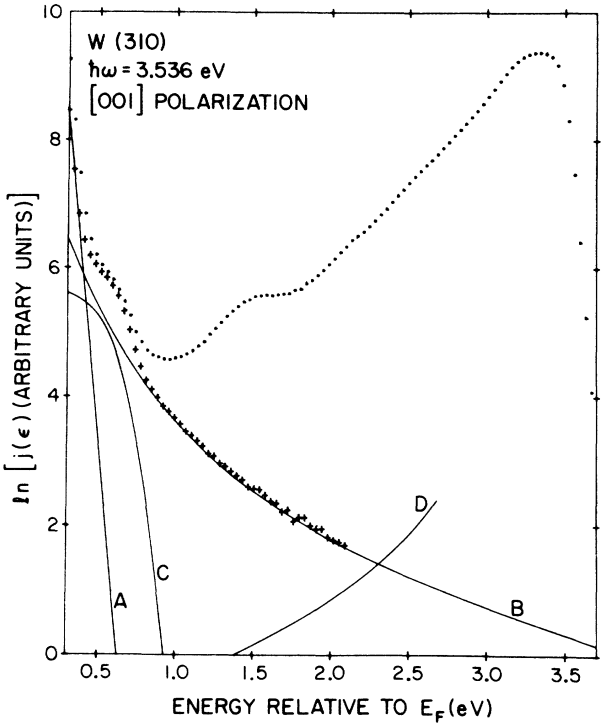

FIG. 2. The TED's measured from the (310) plane of a tungsten field emitter at an applied field of 0.31 V/Å. The crosses (+ + +) are for measurements made in the absence of illumination. The dots (· · · ·) are for measurements made during illumination with 405 nm light at normal incidence. The curves $A-C$ show an approximate decomposition of the high-energy tail of the distribution acquired in the absence of illumination. Curve D is the estimated component due to the low-energy tail of the instrumental function.

To estimate the TED of field emission from the illuminated tip, the TED measured in the absence of illumination must be corrected for the various effects of laser heating. When the tip is illuminated, the strength of component A increases significantly as a result of the temperature-induced increase in the population of states in the energy range above the Fermi level. The temperature rise of the illuminated tip was estimated from the observed increase in current in the first few channels, and the change in component A was deduced by calculating the change in the Fermi-Dirac distribution function.

To first order, temperature changes affect components B and C only indirectly as a result of changes in the total field emission current J_f. Three mechanisms cause J_f to depend on temperature. Firstly, electronic states of higher energy become more highly populated as the temperature increases, and the larger tunneling probability from states of higher energy brings about an increase in

J_f. Secondly, thermal expansion increases the tip radius, which decreases the static electric field at the emitting surface and tends to reduce J_f. Thirdly, the sign and magnitude of the temperature dependence of the intrinsic work function Φ depend upon the plane of observation. The linear coefficients $d\Phi/dT$ applicable close to ambient temperature were taken from the work of Gaudin and Lee.[14] By combining the free-electron theory with the known values of the coefficient of thermal expansion and $d\Phi/dT$, the temperature dependence of the total emission current J_f was estimated. For the data in Fig. 2 this analysis gives a fractional increase in J_f of 1.0%, so illumination of the tip is expected to increase the strengths of components B and C by 2.0% and 1.0% respectively.

The low-energy tail in the photofield emission distribution is due to photoelectrons that lose energy after being field emitted, but before reaching the detector, as a result of inelastic scattering events within the energy analyzer. The strength of this tail was established by measuring the corresponding tail in the field emission TED. At energies sufficiently far below the Fermi energy, only this scattering tail contributes significantly to the field emission TED. In this region the distribution is well described by

$$j_b(\varepsilon)=\gamma J_f|\varepsilon|^{-2.2}, \tag{10}$$

where γ is a constant whose value depends on the alignment of the energy analyzer. The low-energy tail of the TED in photofield emission (labeled D in Fig. 2) was estimated by adopting the value of γ deduced from field emission data, and scaling the resulting distribution by the ratio of the area of the TED in photofield emission to that in field emission.

The data presented in Fig. 2 are typical of experiments performed with the field emitter at close to room temperature. Estimates of the photoemission are reliable only at energies greater than approximately 0.5 eV above the Fermi level, because at lower energies the TED is dominated by the high-energy tail of the field emission TED. For $\varepsilon > 1.0$ eV the Coulomb scattering tail is found to dominate the distribution measured in the absence of illumination. In order to save time during data acquisition, the TED in the absence of illumination was measured to $\varepsilon \simeq 1.6$ eV, and the tail was extrapolated to higher energy by assuming an $\varepsilon^{-2.6}$ dependence, which closely describes its behavior up to $\varepsilon \simeq 4$ eV.[13]

In order to measure the TED in photofield emission over the widest possible energy range, the largest practical electric field was applied so as to minimize the energy dependence of the barrier transmission factor. When measuring emission from low work function planes, the strength of the applied field was reduced so as to ensure that the Coulomb scattering tail of the field emission TED did not dominate the photocurrent. When measuring emission from high work function planes, the strength of the applied field was selected so that the total tip current did not exceed 1 μA, since a larger emission current unduly shortens the lifetime of the tip. In order to minimize the uncertainties inherent in correcting for the high-energy tail of the field emission TED, the conditions of illumination were selected so that the laser-induced tip temperature rise did not exceed 15 K. Figure 3 shows TED's of photofield emission from the (310) and (211) planes respectively, with plane polarized illumination at normal incidence on the emission plane. In typical experimental conditions, the total emission current in field emission was $\sim 10^3$ times larger than that in photofield emission.

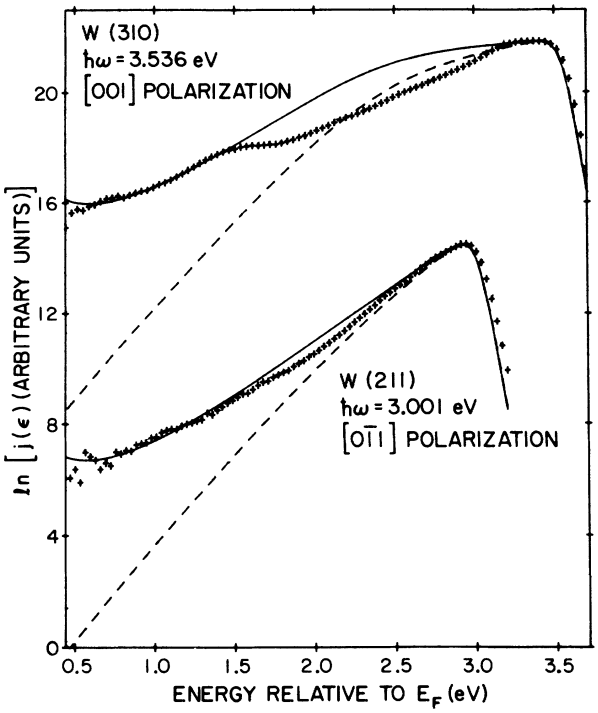

FIG. 3. TED's in photofield emission. The upper curve shows emission from $W(310)$ using 3.536 eV illumination at normal incidence polarized in the [001] direction; the lower curve shows emission from $W(211)$ using 3.001 eV illumination at normal incidence polarized in the [0$\bar{1}$1] direction. In each case the applied field is 0.31 V/Å. The dashed lines are the predictions of the noninteracting gas model evaluated in the free-electron approximation; the solid lines are the predictions of the interacting-gas model evaluated in the free-electron approximation. The two sets of curves have been displaced vertically by arbitrary amounts for clarity.

The experimentally observed TED's were compared with the predictions of the free-electron model. The transmission coefficients for the image-rounded Schottky barrier were computed using Vigneron and Lambin's[15] procedure as extended by Nguyen *et al.*[16] Calculations for the noninteracting electron gas were performed using Eq. (2), and calculations for the interacting electron gas were performed using Eq. (8) extended to finite temperature. To model the effect of instrumental broadening, each of the calculated TED's was convolved with a Gaussian of width 100 meV. TED's predicted by the noninteracting-gas model and by the interacting-gas model evaluated in the free-electron approximation are both plotted in Fig. 3. Neither model contains any free parameters.

In the vicinity of the peak of the TED, the predictions

of both models are consistent with the experimental distributions. However, the variation of the observed photocurrent over the energy range studied is about 400 times stronger than that predicted by the noninteracting-gas model, whereas it is consistent with that predicted by the interacting gas model. The general agreement over several orders of magnitude between the experimental distributions and the predictions of the interacting-gas model is strong evidence that the dominant contribution to the TED in photofield emission in the energy range $0<\varepsilon<\hbar\omega/2$ is due to the emission of electrons from the electron-hole cascade. Exact agreement is not to be expected; the differences between the experimental distributions and the predictions of the interacting-electron-gas model represent departures of the electronic structure of the metal from free-electron form.

In order to remove barrier transmission and thermal effects from the experimentally-observed total energy distribution, and to emphasize those features that yield information about the electronic structure, it is convenient to express experimental TED's in photofield emission in the form of an enhancement factor. Since the electron-hole cascade makes a significant contribution to the TED in photofield emission, it is appropriate to redefine the enhancement factor as

$$R(E)\equiv\ln[j(E)/j_0^*(E)]\ , \tag{11}$$

where j_0^* is the TED calculated on the basis of the interacting-gas model evaluated in the free-electron approximation [Eq. (8)]. By defining the enhancement factor in this way, the strongly energy-dependent secondary electron background is removed.

Total energy distributions in photofield emission from the (111) plane of tungsten in a *s*-polarized light have been measured over a wide range of applied electric field. Figure 4 shows a plot of the enhancement factors deduced from the interacting-gas model, plotted as a function of energy. The data at 0.251 V/Å were acquired approximately one year earlier than the other data; the consistency between the various data sets demonstrates that the enhancement factors are reproducible. To make it easier to compare the various curves, they have been shifted vertically by arbitrary amounts. Even though the ratio $j_p(\varepsilon=3.5\text{ eV})/j_p(\varepsilon=1.6\text{ eV})$, where $j_p(\varepsilon)$ is the total energy distribution in photofield emission, falls from $\sim$4000 to $\sim$20 as the field is increased from 0.196 at 0.316 V/Å, the energy dependence of the enhancement factor is seen to be almost independent of the strength of the applied electric field. This observation implies that the electrons detected at a given energy tunnel through the surface potential barrier *at that energy*. It is further evidence that the anomalous low-energy tail in photofield emission arises from photoelectrons that lose energy as a result of inelastic scattering processes within the field emitter. That the electric field dependence of the enhancement factor is as weak as it is demonstrates that in calculating the enhancement factors the transmission properties of the surface barrier have been treated with reasonable accuracy.

A possible source of the structure observed in the ex-

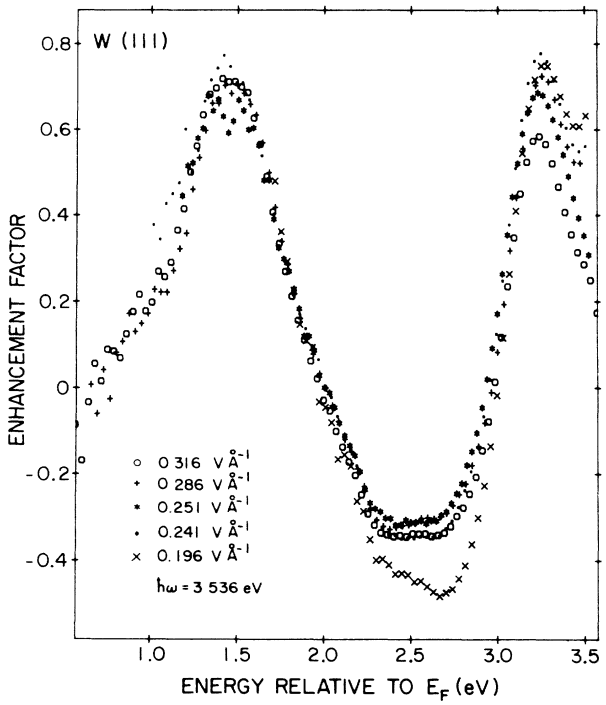

FIG. 4. The enhancement factors based on the interacting gas model derived from $W(111)$ data using 351 nm illumination acquired at five different values of the applied electric field. The curves have been displaced vertically to facilitate comparison.

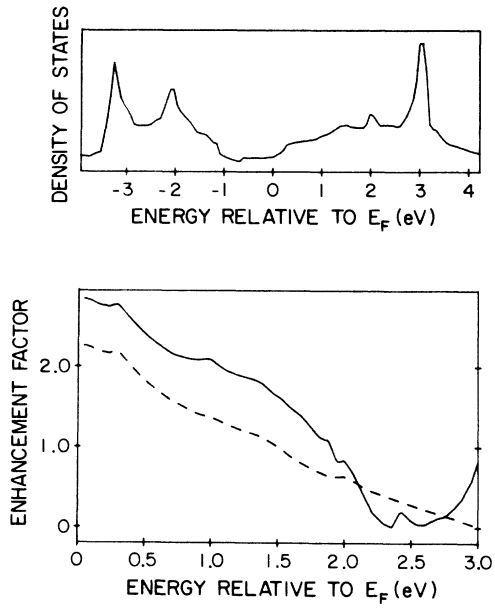

FIG. 5. (a) Density of states of tungsten integrated over the entire Brillouin zone, calculated from a one-electron potential due to Christensen and Feuerbacher (Ref. 17); (b) interacting-gas enhancement factors for tungsten calculated from the bulk DOS in (a), treating electron relaxation in the random-**k** approximation. The solid line is calculated assuming that photoexcitation is proportional to the joint DOS; the dashed line is calculated assuming that photoexcitation is independent of energy.

perimental enhancement factors is that the interacting-gas model in the free-electron approximation may fail to describe with sufficient accuracy the electron-hole cascade. To study this possibility, Kane's method was used to calculate theoretical enhancement factors for tungsten. The energy dependence of the bulk density of states (DOS) was determined from a first-principles band-structure calculation based on a one-electron potential due to Christensen and Feuerbacher[17] [Fig. 5(a)]. Two different model descriptions of the photoexcitation process were studied. In the first it is assumed that photoexcitation is proportional to the joint bulk DOS, which is appropriate if nondirect photoexcitation is dominant. In the second it is assumed that the number of electrons photoexcited to a given energy is independent of energy. The interacting-gas enhancement factors calculated from these two models in the random-**k** approximation are plotted in Fig. 5(b). Although the curve based on the joint bulk DOS calculation shows considerable structure in the range $\varepsilon > \hbar\omega/2$, both calculations show a drop by a factor of about 6 over the entire energy range, with little structure in the range where secondary electrons dominate. On the basis of these results, we conclude that the strong features observed in the experimental enhancement factors cannot be attributed to structure in the distribution of secondary electrons. The interpretation of these features will be discussed elsewhere.[18]

IV. DISCUSSION AND CONCLUSIONS

An anomalous low-energy tail in the TED in photofield emission from tungsten in *s*-polarized light has been observed. On the basis of studies of the strength and the energy and field dependences of the tail, it is attributed to the field emission of secondary electrons from the electron-hole cascade that results from the Auger decay of photoexcited electrons.

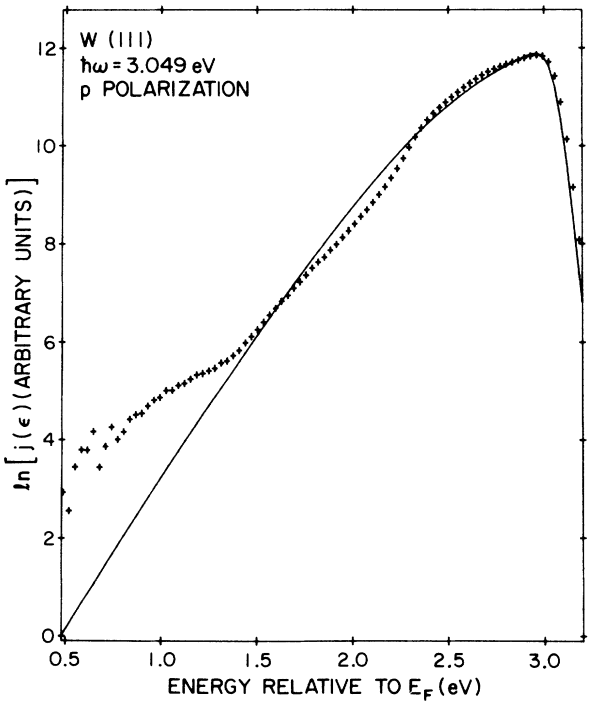

FIG. 6. TED in photofield emission from $W(111)$ using *p*-polarized 3.049 eV illumination at 80° from normal incidence, with an applied field of 0.322 V Å^{-1}. The solid line is the total energy distribution predicted on the basis of a surface-effect model of photofield emission.[20]

No large discrepancies between the experimental data and the predictions of the noninteracting gas model were detected in the work of Venus and Lee.[1] This is because their data were not compared directly with theoretical free-electron distributions, but with parametrized straight-line distributions fitted to the general trend of the data. Moreover, the present data were taken down to lower energies, where the discrepancies are largest, by applying larger electric fields.

The number of electrons and holes per unit energy range in the cascade tail can be estimated by comparing the emission currents observed in photofield emission and field emission. At peak illumination, using light with $\hbar\omega = 3.536$ eV, the ratio j_p ($\varepsilon = 0.5$ ev)$/j_f$ ($\varepsilon = 0.0$ eV) is measured to be on the order of 10^{-6}. The barrier transmission probability at $\varepsilon = 0.5$ eV is approximately 20 times greater than that at the Fermi level. Close to the Fermi level, the densities of electrons and holes with excitation energies ε are expected to be approximately equal, and to have an $\sim\varepsilon^{-4}$ energy dependence. Combining these results, the illumination-induced change in the densities of electrons and holes at peak illumination, expressed as a fraction of the density of electronic states at the Fermi level, is approximately $(3\times10^{-9})\varepsilon^{-4}$, where ε is the excitation energy expressed in eV. At energies more than ~ 0.1 eV above and below the Fermi level, where quasiparticles lose energy primarily by electron-hole pair production, the number of electrons and holes per unit energy range in the cascade is a small fraction of the density of electronic states at the Fermi level.

So far, the discussion has focussed on data taken in *s*-polarized light. In Fig. 6 the TED measured in photofield emission from $W(111)$ using *p*-polarized light incident at 83° from the surface normal, is compared with the predictions of a model of surface photoexcitation from a noninteracting free electron gas.[19,20] Inspection of Fig. 6 shows that the emission at low energy is enhanced over that predicted by the noninteracting free electron model by a factor of approximately 16. Although significant, this enhancement is about 25 times smaller than the corresponding enhancement observed in *s*-polarized light (see Fig. 3). This result supports the idea that the dominant photoexcitation mechanisms in *s*-polarized light and *p*-polarized light are fundamentally different.[1,2]

The origin of the enhanced emission at low energy in *p*-polarized light has not been identified. The enhanced emission might be due to the Auger decay of electrons that are photoexcited in the bulk metal, or it might be due to the Auger decay of electrons that are photoexcited *via* the surface photoelectric effect at the emitting surface and subsequently propagate into the bulk metal. As rough estimates suggest that both of these mechanisms will lead to enhancements of the same order of magnitude as that observed, further study is required to distinguish between them.

An improved experimental study of the cascade tail in photofield emission would require a significant improvement in the signal-to-noise ratio. Reducing the width of the slits of the energy analyzer would almost certainly reduce the noise due to electron scattering within the energy analyzer. The next largest source of noise, the Coulomb scattering tail, could be reduced in relative strength by a factor of two by using a tip with half the radius of curvature. Studies at lower temperature are of particular interest, because within about 0.2 eV of the Fermi level the electron-phonon interaction is expected to replace Auger decay as the dominant mechanism of electronic relaxation, leading to qualitatively new features in the secondary electron distribution.

ACKNOWLEDGMENTS

This research was supported in part by grants from the Natural Sciences and Engineering Research Council of Canada.

[1]D. Venus and M. J. G. Lee, Phys. Rev. B **34**, 4449 (1986).
[2]M. J. G. Lee, Phys. Rev. Lett. **30**, 1193 (1973); Y. Tessieyer, R. Haug, and R. Coelho, Surf. Sci. **87**, 549 (1979); D. Venus and M. J. G. Lee, *ibid.* **125**, 452 (1981).
[3]D. Venus and M. J. G. Lee, Surf. Sci. **172**, 477 (1986).
[4]J. H. Weaver, C. G. Olson, and D. W. Lynch, Phys. Rev. B **12**, 1293 (1975).
[5]P. A. Wolff, Phys. Rev. **95**, 56 (1954).
[6]J. J. Quinn and R. A. Ferrell, Phys. Rev. **112**, 812 (1958); R. H. Ritchie, *ibid.* **114**, 644 (1959); J. J. Quinn, *ibid.* **126**, 1453 (1962); R. W. Davies, *ibid.* **181**, 118 (1969); C. B. Dover and R. H. Lemmer, *ibid.* **183**, 908 (1969).
[7]C. J. Tung and R. H. Ritchie, Phys. Rev. B **16**, 4302 (1977).
[8]R. H. Ritchie, J. Appl. Phys. **6**, 2276 (1966).
[9]J. Lindhard, K. Dan. Vidensk. Mat. Fys. Medd. **28**, 1 (1954).
[10]E. O. Kane, Phys. Rev. **159**, 624 (1967).
[11]I. Lindau and W. E. Spicer, J. Electron Spectrosc. **3**, 409 (1974).
[12]D. Venus and M. J. G. Lee, Rev. Sci. Instrum. **56**, 1206 (1985).
[13]P. J. Donders and M. J. G. Lee, Phys. Rev. B **35**, 6578 (1987).
[14]G. Gaudin and M. J. G. Lee, Surf. Sci. **201**, 540 (1988).
[15]J. P. Vigneron and Ph. Lambin, J. Phys. A **13**, 1135 (1980); Ph. Lambin and J. P. Vigneron, J. Phys. A **14**, 1815 (1981).
[16]H. Q. Nguyen, P. H. Cutler, T. E. Feuchtwang, N. Miskovsky, and A. A. Lucas, Surf. Sci. **160**, 331 (1985).
[17]N. E. Christensen and B. Feurebacher, Phys. Rev. B **10**, 2349 (1974).
[18]P. J. Donders and M. J. G. Lee (unpublished).
[19]A. Bagchi, Phys. Rev. B **10**, 542 (1974).
[20]C. Schwartz and M. W. Cole, Surf. Sci. **115**, 290 (1982).